Soft Matter

Anisotropic Hydrogels formed by Magnetically-Oriented Nanoclay Suspensions for Wound Dressings

Journal:	*Soft Matter*
Manuscript ID	SM-ART-09-2019-001789.R1
Article Type:	Paper
Date Submitted by the Author:	25-Oct-2019
Complete List of Authors:	Yook, Sungho; Purdue University, Materials Engineering Shams Es-haghi, Siamak; Purdue University, Materials Engineering Yildirim, Armen; Purdue University, Materials Engineering Mutlu, Zeynep; Purdue University, Materials Engineering Cakmak, Mukerrem; Purdue University, Materials and Mechanical Engineering Departments

SCHOLARONE™
Manuscripts

Please do not adjust margins

ARTICLE

Anisotropic Hydrogels formed by Magnetically-Oriented Nanoclay Suspensions for Wound Dressings

Received 00th January 20xx,
Accepted 00th January 20xx

DOI: 10.1039/x0xx00000x

Sungho Yook, Siamak Shams Es-haghi, Armen Yildrim, Zeynep Mutlu and Mukerrem Cakmak*

Anisotropic hydrogels are produced, by magnetic alignment of magnetically sensitized nanoclays followed by polymerization of the hydrogel to freeze the developed oriented structure. The anisotropy in these hydrogels is quantitatively investigated using birefringence and 2D Small Angle X-ray Scattering (SAXS) techniques. The oriented nanoclays being intrinsically birefringent provide the optical anisotropy to the hydrogel and this orientation increases with the increase of the applied magnetic field strength. Moreover, 2D SAXS patterns also confirm that the nanoclays are oriented parallel to the permanent magnetic field in a hydrogel with an orientation order parameter of up to 0.67. The field-induced birefringence and 2D SAXS orientation results exhibit a linear correlation over the range of 0 to 9 Tesla (T). The resultant anisotropic hydrogels exhibit substantial swelling anisotropy making them suitable for wound dressings where the out of plane swelling is substantially higher than in-plane swelling to minimize in-plane stress damage to the wounds during healing.

1. Introduction

Nanocomposite hydrogels are the materials which possess nanoparticles within hydrogel networks. By adding nanoparticles into a hydrogel network, additional functionalities such as mechanical strength,[1,2] transparency,[3] swelling kinetics,[4,5] and conductivities[6] can be introduced. Since nanoparticles are randomly dispersed within the three-dimensional (3D) cross-linked network of hydrogels, the structure of nanocomposite hydrogels is usually isotropic. However, the control of nanostructure in hydrogels is often required, for example, to mimic anisotropic mechanical features in natural organisms[7–9] or to fully exploit directional mechanical /optical/electrical properties.[10–12]

Anisotropic swelling is particularly sought after for wound dressing where the vertical wicking of the exudates is preferred because the lateral movement of the fluid to periwound skin may cause maceration through continuing exposure of moisture.[13] Vertical wicking also increases the rate of wound healing by locking the fluid in the core wound.[14] It was reported that the vertical alignment of the superabsorbent nanoparticles in polyurethane reduced the lateral swelling of polyurethane by 33%.[15] It was also shown that the copolymeric gel film exhibited 40% increase of swelling in vertical direction when the side chain of crystal structures were vertically oriented.[16] These reports show that the direction of swelling can be influenced by the oriented nanostructures in hydrogels.

The common approach to fabricating anisotropic nanocomposite hydrogels is to orient colloidal nanoparticles in monomer precursors and arrest the aligned nanoparticles in a cross-linked structure by hydrogelation.[17] To orient nanomaterials in a low viscosity medium before polymerization reaction, the utilization of external shear [18–20] / electric [21–23] / magnetic [10,11,24] fields has been proposed. External electric field is used to orient nanomaterials by taking advantage of permanent or induced dipoles on nanomaterials. Although the precise control and assembly of nanoparticles can be achieved by this method,[25,26] the electrical breakdown in high strength fields and/or electrophoretic migration of nanoparticles are challenging. In contrast, magnetic fields may have an advantage over other external fields as they can be uniformly subjected to materials by non-contact and non-destructive ways without any geometrical constraints.

To orient diamagnetic colloidal nanomaterials by using magnetic force, the energy reduction by the orientation of nanomaterials in the magnetic fields should overcome the thermal energy (k_BT) that can disorder them.[27–29] For the significant free energy reduction in the presence of magnetic fields, the anisotropy of diamagnetic susceptibility in nanomaterials should exists. Although anisotropic 1D or 2D nanoparticles often exhibit anisotropy in the magnetic susceptibility originating from their shape, its value is significantly small for aligning them under magnetic field strengths obtained in ordinary electromagnets. Nevertheless, the alignment of diamagnetic nanoparticles or block copolymers containing aromatic molecules at the field strengths of a few tesla has been reported.[10,29] This has been accomplished by taking advantage of the high anisotropy of diamagnetic susceptibility of rigid aromatic molecules originating from the strong diamagnetic aromatic ring current effect.[30,31] On the other hand, the ferromagnetic nanoparticles (iron, nickel, cobalt) can be aligned in relatively moderate magnetic fields (< 1 Tesla) because they have fairly high magnetic susceptibilities.[32]

Swelling clay minerals are anisotropic natural materials composed of metallic oxides that form layered structures. They can form stable colloidal suspensions in water with negative charge on the surface and exchangeable cations between the interlayers. For this reason, the clay aqueous suspensions can easily be incorporated

School of Materials Engineering, Purdue University, West Lafayette, Indiana 47907, USA, E-mail: cakmak@purdue.edu

† Electronic Supplementary Information (ESI) available: See DOI: 10.1039/x0xx00000x

Please do not adjust margins

into hydrogels.[3,33] Among various types of clay minerals, nontronite is a unique clay mineral which has high levels of ferric ions (Fe^{3+}). It has a similar structure to the montmorillonite clays except that most aluminum ions in the octahedral sheet are replaced by ferric ions. Due to high ferric (III) ion contents in nontronite clays, they are fairly sensitive to magnetic fields. There has been several reports regarding the magnetic orientation of aqueous nontronite minerals[34–36] by using moderate magnetic field strength. However, all subsequent studies were limited to liquid–crystalline behavior of nontronite clay aqueous suspensions. To gain a better understanding of the structure of anisotropic hydrogels which becomes important for practical applications, further quantitative characterization of these materials synthesized under different magnetic field strengths is necessary.

In this work, we demonstrated anisotropic nanoclay hydrogels by arresting magnetically-oriented nontronite nanoclays through the synthesis of hydrogel. The internal anisotropic nanostructure of nanoclay hydrogels was characterized by the measurement of the field-induced birefringence and 2D SAXS. The various anisotropic nanoclay hydrogels were synthesized by controlling the permanent magnetic field strength and nanoclay concentrations. The swelling anisotropy of the resultant hydrogels were also demonstrated.

2. Experimental Section

2.1 Materials

The natural clay mineral (NAu-2) was purchased from Clay Minerals Society at Purdue University. Acrylamide, N,N'-Methylenebis (acrylamide) (MBAA), ammonium persulfate (APS) and N,N,N',N'-Tetramethylethylenediamine (TEMED) were purchased from Sigma-Aldrich and used as received.

2.2 Sample Preparation

Nanoclay preparation. 0.2 g of raw clay minerals (Nau-2) was ground and dispersed in 20 ml of deionized (DI) water by ultrasonication. For the size fractioning, the clay mineral suspension was centrifuged at 15,000 X g for 30 minutes. After large clay particles were precipitated, the supernatant of the solution was collected. The collected supernatant was dried in a vacuum oven overnight and then a powder of nanoclays was obtained. By fractioning size of clay particles, most of impurities in NAu-2 can be removed.[37] The nanoclay aqueous suspensions with different concentrations (0.05 wt%, 0.1 wt%, 0.2 wt% and 0.4 wt%) were prepared by dispersing nanoclays in DI water with ultrasonication. The resultant nanoclays colloidal suspensions were stable over a couple of weeks without any precipitation.

Synthesis of nanoclay hydrogels. Acrylamide (0.15 g) and cross-linker MBAA (0.0075g) were dissolved in the nanoclay aqueous suspension (4.5 g). After complete mixing, the mixture was degassed by bubbling with dry nitrogen gas for 10 mins. Then, the initiator (20mg/ml aqueous solution of APS, 5µL) and catalyst (TEMED, 5µL) were added to the mixture. The mixture was loaded in a 1 ml cylindrical vial or a 4.5ml glass cuvette. The samples were placed in the chamber equipped with a superconducting magnet at 27°C for 90 mins. After 90 mins, the mixture turned into an anisotropic nanoclay hydrogel. By keeping the concentration of monomer, cross-linker, initiator, and catalyst constant, other hydrogels were synthesized by the same procedure with different nanoclay concentrations and magnetic field strength. The magnetic fields were applied to the mixture by using the physical property measurement system (PPMS; Quantum Design). In PPMS, the magnetic field was generated by a superconducting solenoid around the chamber. The solenoid can generate a vertical magnetic field in the chamber up to 9 Tesla.

2.3 Methods

Powder X-ray diffraction. Nanoclay samples after fractioning size were ground with mortar and pestle and packed in an X-ray sample holder. Powder X-ray diffraction data were collected on a Bragg–Brentano diffractometer (Panalytical Empyrean) with a CuKα radiation (1.541 Å). X-ray Data were collected between 5° and 90° using the Panalytical Data Collector software.

Birefringence measurements. The birefringence was measured by a custom-built machine utilizing automated birefringence system. The details about the design and capabilities of this machine can be found elsewhere.[38] Briefly, this machine can measure various properties of materials including optical retardation (birefringence) and transmission. The in-plane retardation was obtained by subtracting initial retardation of isotropic hydrogel sample from the retardation of the anisotropic hydrogel samples. Then the birefringence was simply calculated by dividing the in-plane retardation with respect to sample thickness as shown by

$$\Delta n_{12} = \frac{Retardation}{thickness} \qquad (1)$$

2D SAXS measurements. The anisotropic nanoclay hydrogels were prepared in the glass capillary with closed ends (1.5mm diameter, 0.01mm wall thickness) to carry out 2D SAXS experiment. SAXS experiments were performed by an Anton Paar SAXSpoint 2.0. X-ray beam with monochromatized CuKα radiation (1.541 Å) was used for the experiments. The sample to detector distance was 1.075 m and the X-ray exposure time was 30 minutes for each sample. The azimuthal plots were constructed by integrating the intensity of the scattering patterns from q = 0.07nm-1 to q = 0.45 nm-1 for every 1° by using SAXS analysis software offered by Anton Paar.

Rheological measurements: The viscosity of hydrogel precursor solution was measured by using a rheometer (Bohlin Gemini HR Nano 200) at room temperature during the polymerization reaction. The viscosity of solution was observed with time at constant shear rate (10 s^{-1}).

Transmission Electron Microscopy (TEM): The 0.01 wt% nanoclay aqueous suspension was prepared by ultrasonication. One drop of the solution was dropped on the TEM copper grid and the sample was dried. Nanoclays were observed by using a Tecnai T20 TEM at 200 kV.

Compression Tests: The non-oriented and oriented cylindrical hydrogels with 9 mm diameter and 5 mm height were prepared with a series of clay concentrations (0.05wt%, 0.2wt%, 0.4wt%). The stress-strain curve of each sample was obtained under uniaxial compression by using DMA 850 (TA Instruments). The constant displacement rate (1 mm/min) was applied for the measurement.

Water Swelling Tests: For swelling measurements of nanoclay hydrogels, seven different cylindrical samples with 9 mm diameter and 5 mm height were prepared with 0.4 wt% hydrogels with

This journal is © The Royal Society of Chemistry 20xx

oriented (9 T) and non-oriented (0 T) nanoclays. The diameter, height and weight of the samples before and after the room temperature water swelling were measured for various swelling time intervals. The changes in dimensions and weight before and after swelling were measured with a caliper (0.01 mm resolution) and a balance (0.1 mg resolution), respectively. The percentage increase of the length of diameter and height were calculated along with weight percentage increase.

3. Results and Discussion

Nontronite clays (NAu-2) are dioctahedral minerals containing ferric ions (Fe^{3+}) in octahedral sheet (Fig. 1a). The shape and size of nontronite nanoclays were determined by TEM observation. Most of nontronite nanoclays appeared as rectangular nanosheets in TEM images, probably due to perpendicular orientation of clay nanosheets to the electron beam direction (Fig. 1b). The average length and width of nanosheets were 209 nm and 77 nm, respectively (ESI,† Fig. S1). The crystal structure of NAu-2 was investigated by a powder X-ray diffraction (Fig. 1c). Normally, the nontronite clay shows two major peaks at $2\theta = 6°$ and $2\theta = 28°$ from (001) and (003) plane reflection, respectively.[39,40] Fig. 1c clearly shows these two reflections. There are also two distinct peaks at $2\theta = 19.5°$ and 35° indicating (20,11) and (20,13) peaks, which were attributed to dioctahedral 2:1 layer stacking faults of nontronite clays.[41,42] Fig. 1d shows the overall sample preparation steps of an anisotropic clay hydrogel by using a permanent superconducting magnet. Briefly, the nontronite aqueous suspension with hydrogel precursor (monomer, crosslinker, initiator, and catalyst) was prepared in a container. The nanoclays in the mixture were aligned by placing the solution in a superconducting magnet. The following hydrogelation in the presence of the magnetic field immobilizes the oriented nanoclays within the hydrogel. To find out the optimal exposure time of the magnetic fields to low viscous liquid medium before a polymerization, the viscosity of hydrogel precursor solution was measured as a function of time at room temperature during polymerization (ESI,† Fig. S2). By adding 5μL of initiator and catalyst to 4.5 g of water, we tuned the onset of viscosity rise to 40 min. This result indicated that the nanoclay suspensions were exposed to magnetic fields in the liquid medium approximately for 40 mins and then the polymerization took place to freeze the developed morphology within the structure. Although the real-time nanoclay alignment and monomer gelation kinetics could not be studied due to geometrical restriction, the nanoclay alignment would probably be relatively fast in a liquid state considering the water-like viscosity of the medium. The exposure to the permanent magnetic fields for 40 mins in the liquid state should be enough for nanoclays to be oriented at the corresponding magnetic field strengths used.

Fig. 2a shows cylindrical anisotropic hydrogels with different clay concentrations prepared under the 9 T magnetic field. The resultant nanoclay hydrogels exhibited uniform color from light yellow to dark brown as the concentrations of nanoclays increased from 0.05 wt% to 0.4 wt%. In this study, we report nanoclay hydrogels with relatively low nanoclay concentrations to solely consider the orientation of nanoclay in isotropic aqueous suspension. One of the important features of nontronite clay minerals is that they can exhibit yield stress in aqueous state.[43,44] Because of this characteristic, nontronite nanoclay suspensions can undergo an isotropic/nematic and a sol/gel transition as the overall clay concentration increases. For nontronite clays (Nau-2) aqueous suspensions, isotropic/nematic and sol/gel transitions occur at 0.6 vol% and 0.83 vol%, respectively.[36] Therefore, the results presented in this study deal with isotropic liquid region to exclude a gelation caused by high clay loading. This means that the hydrogelation of clay suspensions in this report only occurred by a polymerization of acrylamide monomers. For examining the magnetic field-induced nanoclay alignment in hydrogels, the birefringence of the materials was characterized. This technique is suitable for tracking preferential orientation of optically anisotropic particles and other materials.[45] Nontronite nanoclays are inherently birefringent as their refractive indices in the basal plane direction and normal to the basal plane directions are substantially different. Thus, hydrogel nanocomposite can be optically birefringent when nanoclays are preferentially oriented. For this measurement, the anisotropic hydrogel samples were placed between cross polarizers and the optical anisotropy was characterized by observing the light intensity at every 45° rotation as shown in Fig. 2b. For the nanoclay hydrogel exposed to a relatively low magnetic field of 1 T, the light transmission intensity changes at every 45° rotation was low (Fig. 2 c1). This increased for the sample prepared at 3 T magnetic field strength (Fig. 2 c2). Notably, the strong dark and bright contrast was observed for the sample prepared at the magnetic strength of 9 T as the clays became oriented. (Fig. 2 c3). To verify that optical anisotropy was only from field-induced orientation of nanoclays not from polymer chains of hydrogel network, the optical anisotropy of pure hydrogels prepared in 9 T was examined (ESI,† Fig. S3). Completely dark polarized optical microscopy (POM) images at every 45° rotation indicated that a hydrogel is optically isotropic. The orientation direction of nanoclays with respect to the direction of the magnetic fields was revealed by inserting a first order lambda plate (red wave plate) between cross polarizers with its slow axis oriented at 45 degrees to the polarizer and analyzer. With a red wave plate, the sample exhibited the contrast interference colors (red → yellow → red → blue) at every 45° rotation (Fig. 2 c4). Blue interference color appeared at 135° rotation when applied magnetic field direction was parallel to slow axis direction of the lambda plate, whereas yellow color appeared at 45° rotation as shown in Fig. 2d (slow axis direction of the red wave plate is indicated by red double arrow in these figures). The result indicates that (001) basal planes, which have a high refractive index in nanoclay minerals, oriented along the applied magnetic field direction. Thus, blue color (a high refractive index in Michel-Levy Birefringence Chart) exhibited when the (001) basal planes are oriented parallel the slow axis (= highest refractive index direction) of the first-order (red wave) lambda plate.

For a more detailed examination of the magnetic-field induced birefringence, nanoclay hydrogel samples were prepared in a 4.5 ml glass cuvette with different magnetic field strength and concentrations. Nanoclay hydrogels optically look similar to each other at the same clay concentrations without cross polarizers (Fig. 3a). However, the samples gradually became bright between cross polarizers as the magnetic field strength increased because of preferential orientation of nanoclays (Fig. 3b). The gradual enhancement of birefringence intensity was observed for the

concentration from 0.05 wt% to 0.2 wt%, while the effect was not significant for 0.4 wt% nanoclay hydrogel samples.

To evaluate the birefringent intensity quantitatively, the in-plane retardation of the samples was measured by using a custom-built apparatus. The scheme of the experimental set-up and relevant in-plane retardation values are shown in ESI,† Fig. S4. Fig. 4 presents the magnetic-field induced birefringence of nanoclay hydrogels as a function of magnetic field strength. As expected, the field-induced birefringence of nanoclay hydrogels increased with magnetic field strength in all nanoclay concentrations. Interestingly, the birefringence increased with nanoclay concertation from 0.05 wt% to 0.2 wt%, then it dropped when concentration increased to 0.4 wt% at the same magnetic field strength. For dilute colloidal system, the field-induced birefringence is linearly proportional to particle concentrations as expressed by

$$\Delta n = \Delta n_{sat} C_V S \qquad (2)$$

where C_v is a volume concentration of particles, S is an orientation order parameter and Δn_{sat} is a maximum birefringence when C_v =1 and S =1.[46,47] The field-induced birefringence is dependent on the orientation order parameter (S) with constant C_v and Δn_{sat}. Thus, birefringence is proportional to magnetic field strength at the constant nanoclay concentration as orientation order parameter (S) increased. Similarly, the field-induced birefringence was increased with nanoclay concentration from 0.05 wt% to 0.2 wt% at the constant external field strength. However, this equation is only applied for the dilute nanoclay suspensions, where individual nanoclays can independently contribute to the field-induced birefringence by orientating in the field direction without geometric hindrance. For the sample with high nanoclay loading like 0.4 wt% in this study, the nanoclay particles do not act individually anymore as they interfere with the motion of neighboring particles and hence restricting their free realignment. Hence, the overall orientation of the particles decrease slightly because of this spatial restriction effect at higher concentrations.

The anisotropic structure of nanoclay hydrogels was also examined by 2D SAXS analysis. The X-ray beam was directed perpendicular to the applied magnetic field direction as shown in Fig. 5a. Fig. 5b shows that 2D SAXS patterns of nanoclay hydrogels (0.1 wt%, nanoclay) prepared with different magnetic field strength. As applied magnetic field increased from 0 T to 9 T, the shape of X-ray scattering pattern changed from circular to elliptical shape. The longer axis of elliptical pattern, which was perpendicular to the direction of applied magnetic fields indicating that the basal plane of nanoclays were oriented parallel to the direction of applied magnetic fields. This result was also in agreement with POM image with the lambda (red wave) plate (Fig. 2c-4). To clarify the degree of the alignment, the azimuthal plot of 2D SAXS patterns in fig. 5b was constructed (Fig. 5d). The plot of the sample with 0 T showed a single plateau along the azimuthal angles. As the applied magnetic fields increased, two distinct peaks at 90° and 270° azimuthal angles was getting pronounced. The results clearly indicate the nanoclay hydrogels increasingly become anisotropic as magnetic field strength increased. Furthermore, the elliptical 2D SAXS patterns were observed in all samples prepared at the 9 T magnetic field strength (Fig. 5 b4 and c1 - c3). The constructed azimuthal plot of 2D SAXS patterns in Fig. 5c exhibited strong intensity at 90° and 270° azimuthal angle in all samples, indicating high alignment of nanoclays in all concentrations (Fig. 5e). To verify that the X-ray scattering is from nanoclay structure, the X-ray scattering pattern of the pure hydrogel was examined (Fig. 5c-4). The negligible scattering intensity of the pure hydrogel indicates that the X-ray scattering patterns are from nanoclays not from the hydrogel matrix.

To quantitatively analyze the nanoclay orientation, the orientation order parameters (S) were calculated by fitting the azimuthal angle plots to the Maier-Saupe distribution function with a base line and the positions of maximum intensity (90° and 270° in this study). By fitting the plot to the function, we can obtain a parameter (α) that determines the width between two peaks. This width parameter (α) was used to calculate the orientation order parameter. Theoretically, the value of S ranges from 1 (perfect orientation) to 0 (completely random orientation). The detailed calculation method is described elsewhere.[48,49] The orientation order parameters of the nanoclay hydrogel (0.1 wt%) increased gradually by increasing the magnetic field strength (Fig. 6a). The orientation parameter increased along with the magnetic field strength up to 5 T (from 0 to 0.6). This increase slows down with further increase of magnetic field to 9 T (from 0.6 to 0.68). Fig. 6b shows the orientation order parameter of nanoclay hydrogels prepared at 9 T with different clay concentrations. For the low concentration samples (0.05wt% and 0.1wt%), the orientation order parameter takes high values ~ 0.68. It slightly decreased to 0.6 as the concentration of nanoclays increased to 0.2 wt%. However, a further increase in the concentration significantly reduced the orientation order parameter down to 0.43 (0.4 wt%). The result agreed with the decrease in the field-induced birefringence for the sample with high clay loading (0.4 wt%). The plot in Fig. 6c shows expected linear correlation between the field-induced birefringence and the orientation order parameter obtained from 2D SAXS over the magnetic field strength ranged from 0 T to 9 T.

The mechanical properties of nanoclay hydrogels were also investigated along the clay orientation direction at different concentrations. The nanoclay hydrogels showed the typical stress-strain curve of hydrogel materials under compression test (Fig. 7a). In general, modulus with nanoclay concentration increased even though the clay concentrations we used was quite small. Moreover, anisotropic hydrogels showed slightly enhancement in mechanical properties in the clay orientation direction at 50 % strain (testing was carried out in normal direction). In all concentrations, the tangent elastic modulus of anisotropic hydrogels was higher than that of isotropic hydrogels at 50% strain (Fig. 7b). For the 0.4 wt% hydrogels, tangent elastic modulus was increased from 15.4 kPa to 18.1 kPa, which corresponding to 18% increase in mechanical properties. The tangent elastic modulus also increased as the concentration of nanoclay concentration increased for both non-oriented and oriented samples.

Lastly, we examined the swelling behavior of the hydrogels with 0.4 wt% nanoclays with the oriented and non-oriented samples. The initial and final dimensions of the sample were measured at different swelling times as shown in Fig. 8a. We observed that anisotropic hydrogels exhibited high swelling in the direction of orientation of nanoclays. Fig. 8b shows that the percentage increase of diameter and height along with weight percentage change over the swelling

This journal is © The Royal Society of Chemistry 20xx

time. At equilibrium swelling state of hydrogel where 60% increase in weight of the hydrogel after 120 h swelling was observed, the thickness and diameter increased 30% and 21%, respectively. However, swelling % in the radius and thickness direction was almost identical over time for the sample without the clay orientation (Fig. 8c). The results indicated that the oriented nanoclay in a hydrogel network facilitated the anisotropic water swelling over time. Anisotropic swelling ratio (Y% / X%) was plotted over time for the oriented and non-oriented samples in Fig. 8d. The results show that the hydrogels with oriented nanoclays maintained anisotropic swelling (~1.5) after 6h, whereas the hydrogels with non-oriented nanoclays exhibited no anisotropy swelling for all swelling times.

Table 1 shows the swelling anisotropy of polymeric gels in ethanol or water in previous studies. Based on previous findings, the anisotropic swelling exhibited up to 1.4 in ethanol and 1.3 in water with polymeric gels containing anisotropic nanostructure. Here, we report the swelling anisotropy (~1.5) in water which is the highest among the published literature.

Table 1 Anisotropic swelling of polymeric gels

Materials (Gel)	Swelling Solvent	Anisotropic Swelling
Copolymer of Stearyl acrylate and acrylic acid[16]	Ethanol	1.4
Polyurethane[15]	Water	1.25
Poly(N-isopropylacrylamide)[20]	Water	1.3
Polyacrylamide*	Water	1.5

* The material used in this study

4. Conclusions

We produced a new type of anisotropic nanocomposite hydrogels by using a magnetic alignment of iron containing magnetically sensitized clays in the field direction potentially useful for wound dressings that exhibit substantial out of plane wicking behavior. Anisotropic nanostructure of nanoclay hydrogels was investigated by measuring birefringence and SAXS. The field-induced birefringence and 2D SAXS results revealed that nanoclay suspensions within a hydrogel were oriented parallel to the magnetic field direction and the degree of orientation nanoclays was increased with applied magnetic field strength. Interestingly, nanoclays were less responsive to external fields beyond a certain clay loading where the strong steric hindrance was observed between clay particles forming frustrated structures. In these structures, the improved compressive mechanical properties as well as the increases in swelling behavior were found in the direction of nanoclay orientation facilitated by the magnetic field.

Conflicts of interest

There are no conflicts of interest to declare.

Acknowledgements

Partial support for this work was provided by NSF (# 1511896) for which the authors are grateful.

References

1 Q. Wang, J. L. Mynar, M. Yoshida, E. Lee, M. Lee, K. Okuro, K. Kinbara and T. Aida, *Nature*, 2010, **463**, 339–343.
2 K. Haraguchi and H. J. Li, *Macromolecules*, 2006, **39**, 1898–1905.
3 K. Haraguchi, T. Takehisa and S. Fan, *Macromolecules*, 2002, **35**, 10162–10171.
4 J. Zhang and A. Wang, *React. Funct. Polym.*, 2007, **67**, 737–745.
5 J. Mu and S. Zheng, *J. Colloid Interface Sci.*, 2007, **307**, 377–385.
6 X. Zhao, X. Ding, Z. Deng, Z. Zheng, Y. Peng and X. Long, *Macromol. Rapid Commun.*, 2005, **26**, 1784–1787.
7 D. L. Thomsen, P. Keller, J. Naciri, R. Pink, H. Jeon, D. Shenoy and B. R. Ratna, *Macromolecules*, 2001, **34**, 5868–5875.
8 V. C. Mow and X. E. Guo, *Annu. Rev. Biomed. Eng.*, 2002, **4**, 175–209.
9 A. Ní Annaidh, K. Bruyère, M. Destrade, M. D. Gilchrist and M. Otténio, *J. Mech. Behav. Biomed. Mater.*, 2012, **5**, 139–148.
10 L. Wu, M. Ohtani, M. Takata, A. Saeki, S. Seki, Y. Ishida and T. Aida, *ACS Nano*, 2014, **8**, 4640–4649.
11 M. Liu, Y. Ishida, Y. Ebina, T. Sasaki, T. Hikima, M. Takata and T. Aida, *Nature*, 2015, **517**, 68–72.
12 Y. S. Kim, M. Liu, Y. Ishida, Y. Ebina, M. Osada, T. Sasaki, T. Hikima, M. Takata and T. Aida, *Nat. Mater.*, 2015, **14**, 1002–1007.
13 K. Y. Woo, D. Beeckman and D. Chakravarthy, 2017, **30**, 494–501.
14 D. Okan, M. Student, K. Woo, W. H. Clinic, E. A. Ayello, S. Advisor, C. A. Editor, W. Care, R. G. Sibbald, P. H. Sciences, W. H. Clinic, C. A. Editor and W. Care, *Adv. Skin Wound Care*, 2007, **20**, 39–53.
15 Y. Guo, S. Pan, F. Jiang, E. Wang and L. Miinea, *RSC Adv.*, 2018, **8**, 8173–8180.
16 E. S. Limited, *Polym. Gels Networks*, 1998, **5**, 429–438.
17 K. Sano, Y. Ishida and T. Aida, *Angew. Chemie - Int. Ed.*, 2018, **57**, 2532–2543.
18 X. Y. Lin, Z. J. Wang, P. Pan, Z. L. Wu and Q. Zheng, *RSC Adv.*, 2016, **6**, 95239–95245.
19 Z. Zhu, Y. Li, H. Xu, X. Peng, Y. N. Chen, C. Shang, Q. Zhang, J. Liu and H. Wang, *ACS Appl. Mater. Interfaces*, 2016, **8**, 15637–15644.
20 N. Miyamoto, M. Shintate, S. Ikeda, Y. Hoshida, Y. Yamauchi, R. Motokawa and M. Annaka, *Chem. Commun.*, 2013, **49**, 1082–1084.
21 T. Inadomi, S. Ikeda, Y. Okumura, H. Kikuchi and N. Miyamoto, *Macromol. Rapid Commun.*, 2014, **35**, 1741–1746.
22 S. Batra, E. Unsal and M. Cakmak, *Adv. Funct. Mater.*, 2014, **24**, 7698–7708.
23 Y. Guo, Y. Chen, E. Wang and M. Cakmak, *ACS Appl. Mater.*

Interfaces, 2017, **9**, 919–929.

24 J. E. Kim, T. H. Han, S. H. Lee, J. Y. Kim, C. W. Ahn, J. M. Yun and S. O. Kim, *Angew. Chemie - Int. Ed.*, 2011, **50**, 3043–3047.

25 Z. Hu, M. D. Fischbein, C. Querner and M. Drndić, *Nano Lett.*, 2006, **6**, 2585–2591.

26 K. M. Ryan, A. Mastroianni, K. A. Stancil, H. Liu and A. P. Alivisatos, *Nano Lett.*, 2006, **6**, 1479–1482.

27 T. Kimura, T. Uemura, T. Kimura, S. Takagi and H. Inoue, *Macromol. Symp.*, 2006, **242**, 120–125.

28 M. Eguchi, M. S. Angelone, H. P. Yennawar and T. E. Mallouk, *J. Phys. Chem. C*, 2008, **112**, 11280–11285.

29 M. Gopinadhan, P. W. Majewski, E. S. Beach and C. O. Osuji, *ACS Macro Lett.*, 2012, **1**, 184–189.

30 P. Stamenov and J. M. D. Coey, *J. Magn. Magn. Mater.*, 2005, **290–291**, 279–285.

31 G. P. Charbonneau and P. Rivet, *Acta Crystallogr. Sect. A*, 1980, **36**, 51–53.

32 Y. Chen, Y. Guo, S. Batra, E. Wang, Y. Wang, X. Liu, Y. Wang and M. Cakmak, *Nanoscale*, 2015, **7**, 14636–14642.

33 O. Okay and W. Oppermann, *Macromolecules*, 2007, **40**, 3378–3387.

34 C. Abrahamsson, L. Nordstierna, M. Nordin, S. V. Dvinskikh and M. Nydén, *J. Colloid Interface Sci.*, 2015, **437**, 205–210.

35 M. MacGregor-Ramiasa, C. Abrahamsson, M. Röding and M. Nydén, *Appl. Clay Sci.*, 2015, **116–117**, 167–174.

36 L. J. Michot, I. Bihannic, S. Maddi, S. S. Funari, C. Baravian, P. Levitz and P. Davidson, *Proc. Natl. Acad. Sci.*, 2006, **103**, 16101–16104.

37 J. L. Keeling, M. D. Raven and W. P. Gates, *Clays Clay Miner.*, 2000, **48**, 537–548.

38 E. Unsal, J. Drum, O. Yucel, I. I. Nugay, B. Yalcin and M. Cakmak, *Rev. Sci. Instrum.*, 2012, **83**, 025114.

39 Y. L. Li, H. Vali, S. K. Sears, J. Yang, B. Deng and C. L. Zhang, *Geochim. Cosmochim. Acta*, 2004, **68**, 3251–3260.

40 D. Liu, H. Dong, M. E. Bishop, J. Zhang, H. Wang, S. Xie, S. Wang, L. Huang and D. D. Eberl, *Geobiology*, 2012, **10**, 150–162.

41 C. Tchoubar, *J. Appl. Crystallogr.*, 1983, **16**, 374–383.

42 W. P. Gates, P. G. Slade, A. Manceau and B. Lanson, *Clays Clay Miner.*, 2002, **50**, 223–239.

43 P. Coussot, Q. D. Nguyen, H. T. Huynh and D. Bonn, *Phys. Rev. Lett.*, 2002, **88**, 1755011–1755014.

44 B. Abou, D. Bonn, J. Meunier and J. Meunier, *J. Rheol. (N. Y. N. Y).*, 2003, **47**, 979.

45 B. R. Jennings, S. R. Wilson and P. J. Ridler, *J. Colloid Interface Sci.*, 2005, **281**, 368–376.

46 T.-Z. Shen, S.-H. Hong and J.-K. Song, *Nat. Mater.*, 2014, **13**, 394–9.

47 I. Dozov, E. Paineau, P. Davidson, K. Antonova, C. Baravian, I. Bihannic and L. J. Michot, *J. Phys. Chem. B*, 2011, **115**, 7751–7765.

48 S. Feng, X. Xiong, G. Zhang, N. Xia, Y. Chen and W. Wang, *Macromolecules*, 2009, **42**, 281–287.

49 Y. Nie, G. Huang, L. Qu, X. Wang, G. Weng and J. Wu, *Polymer*, 2011, **52**, 3234–3242.

This journal is © The Royal Society of Chemistry 20xx

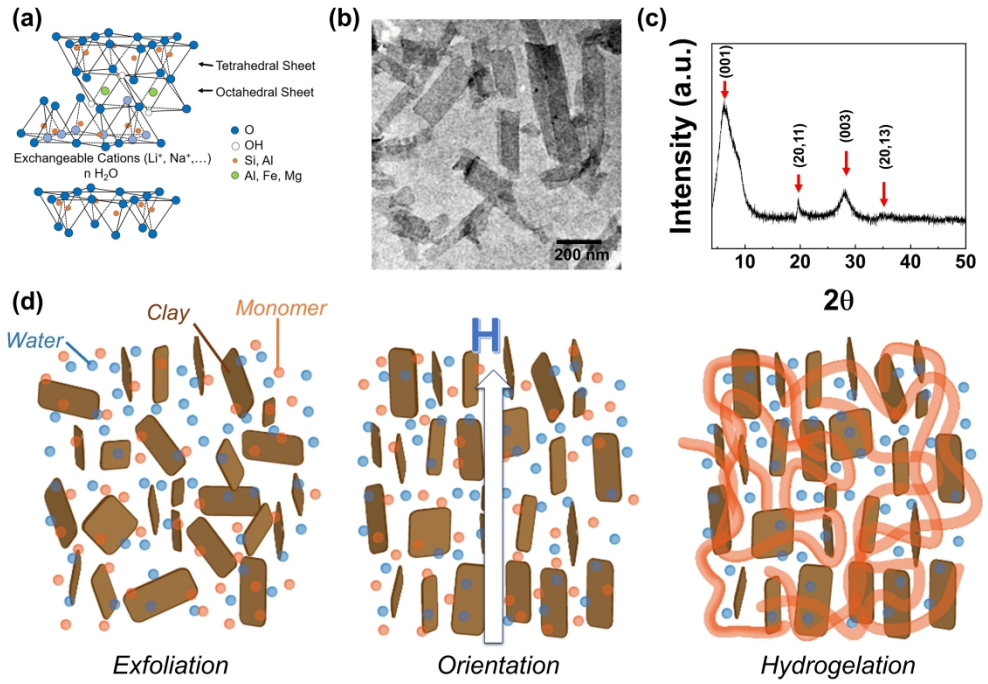

Fig. 1 (a) The structure of nontronite clay (NAu-2). (b) TEM image of nontronite nanoclays. (c) X-ray diffraction patterns of nontronite nanoclays. (d) Schematic illustration of preparation process of an anisotropic clay hydrogel sample.

393x279mm (300 x 300 DPI)

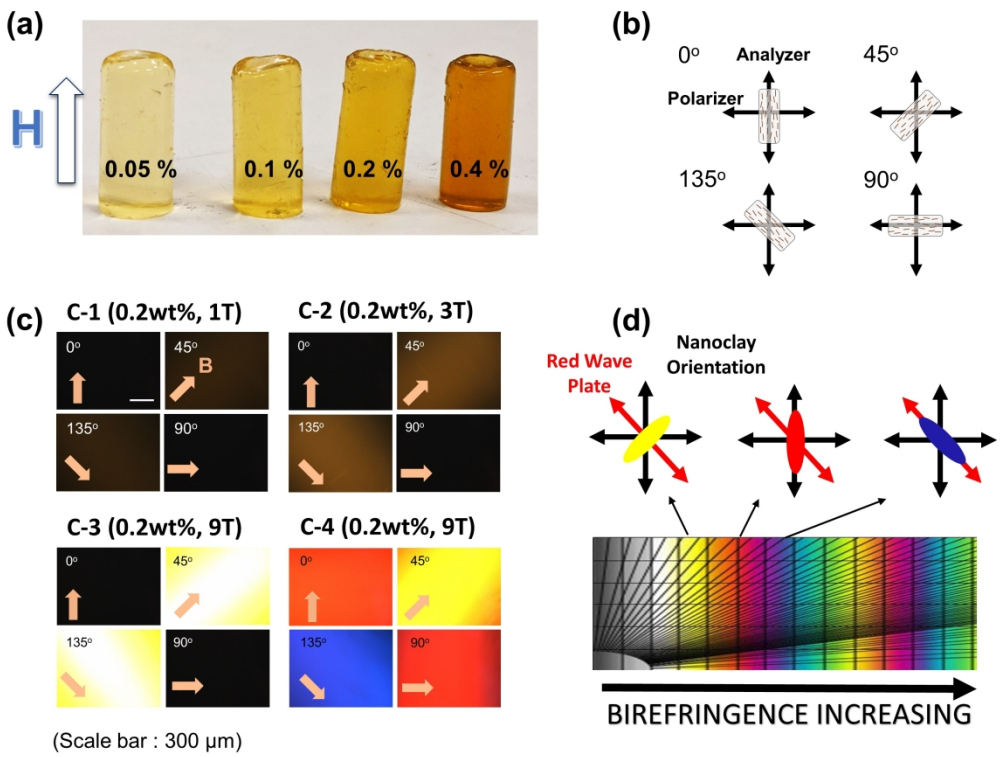

Fig. 2 (a) Anisotropic hydrogels with different concentrations of nanoclay (0.05 wt%, 0.1 wt%, 0.2 wt%, 0.4 wt%) prepared under 9 T magnetic field. (b) The direction of the sample rotation between cross polarizers. (c) The optical microscope image of 0.2 wt % anisotropic hydrogels prepared at (c-1) 1 T, (c-2) 3 T, and (c-3) 9 T of magnetic field strength under cross polarizers. (c-4) Identical POM image of (c-3) with a first order lambda plate (red wave plate) (scale bar : 300 μm) (d) Nanoclay orientation under cross-polarizers with a red wave plate and a corresponding interference color chart

271x210mm (300 x 300 DPI)

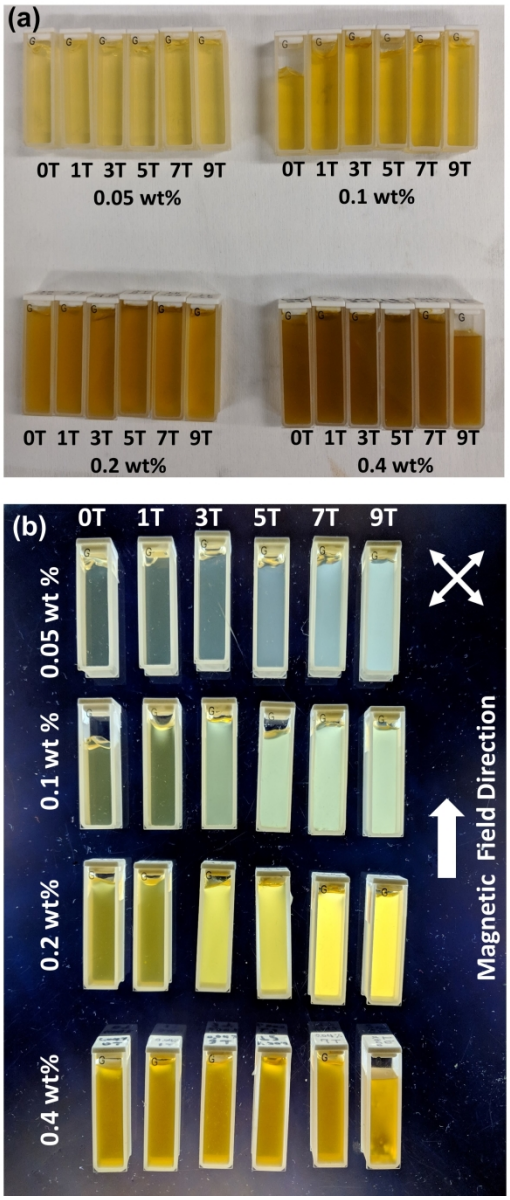

Fig. 3 Anisotropic hydrogel samples (0.05 wt%, 0.1 wt%, 0.2 wt%, 0.4 wt% of nontronite clays) prepared with various magnetic field strength (0, 1, 3, 5, 7, 9 Tesla) (a) without cross polarizers and (b) with cross polarizers.

157x368mm (300 x 300 DPI)

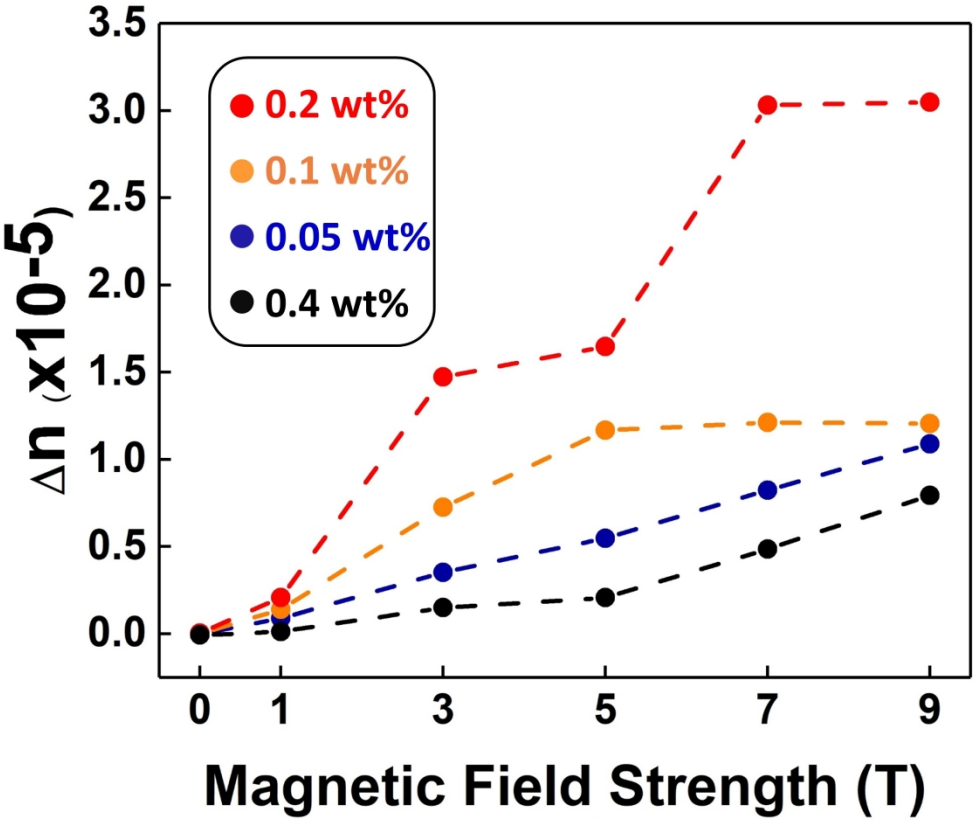

Fig. 4 Magnetic-field induced birefringence of anisotropic nanoclay hydrogels.

228x190mm (300 x 300 DPI)

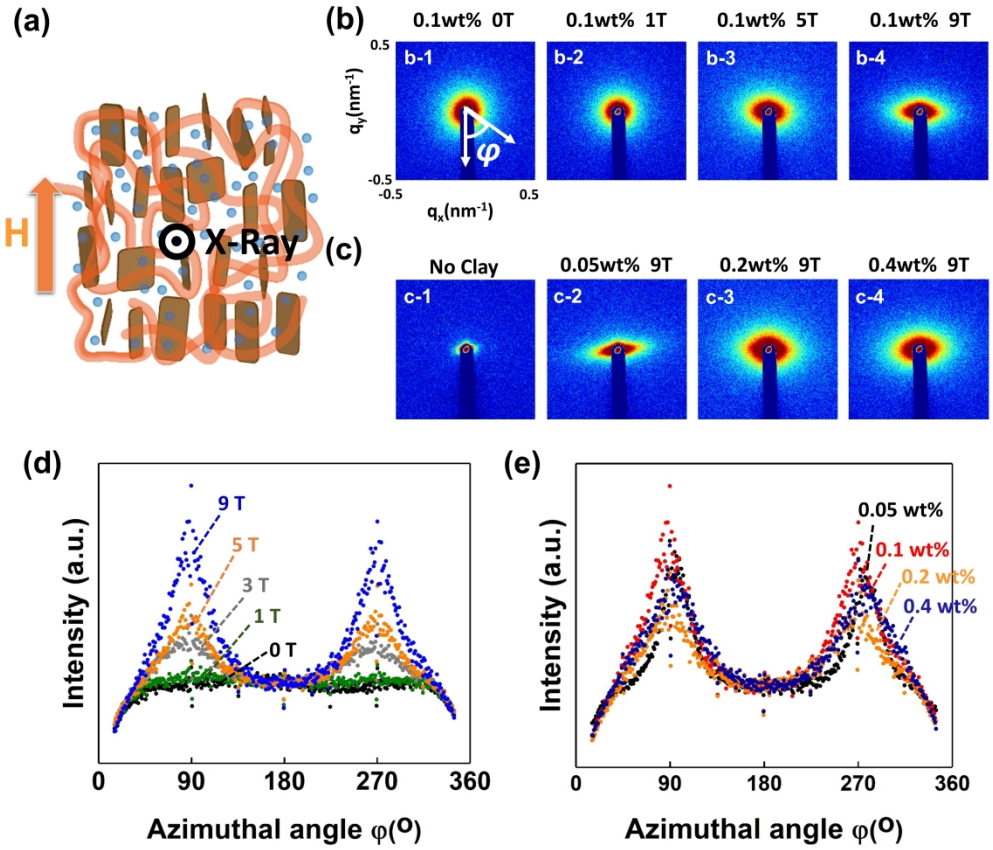

Fig. 5 (a) Schematic illustration of nanoclay hydrogels along with x-ray beam direction and applied magnetic field direction (b) 2D SAXS patterns of hydrogels (0.1 wt%) in different magnetic field strength. (c) 2D SAXS patterns of hydrogels in different clay concentration prepared at 9 T magnetic field. (d) Azimuthal angle plots for hydrogels (0.1 wt%) in different magnetic fields. (e) Azimuthal angle plots for anisotropic hydrogels in different concentrations prepared in 9 T magnetic fields

317x279mm (300 x 300 DPI)

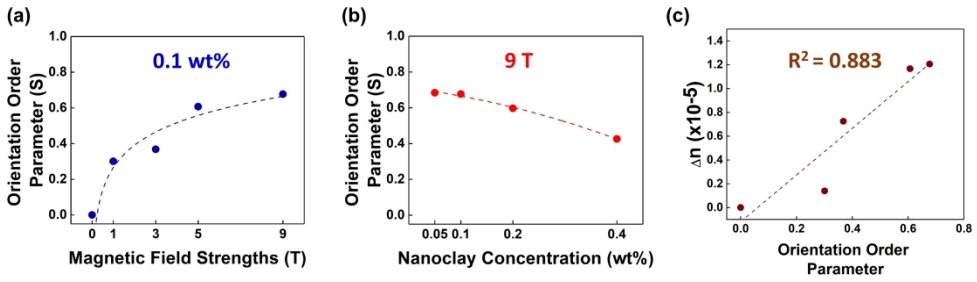

Fig. 6 (a) The orientation order parameter of 0.1 wt% nanoclay hydrogels as a function of the magnetic field strength. (b) The orientation order parameter of nanoclay hydrogels as a function of nanoclay concentration. (c) The correlation between birefringence and orientation order parameter (0.1 wt% nanoclay hydrogels).

426x119mm (300 x 300 DPI)

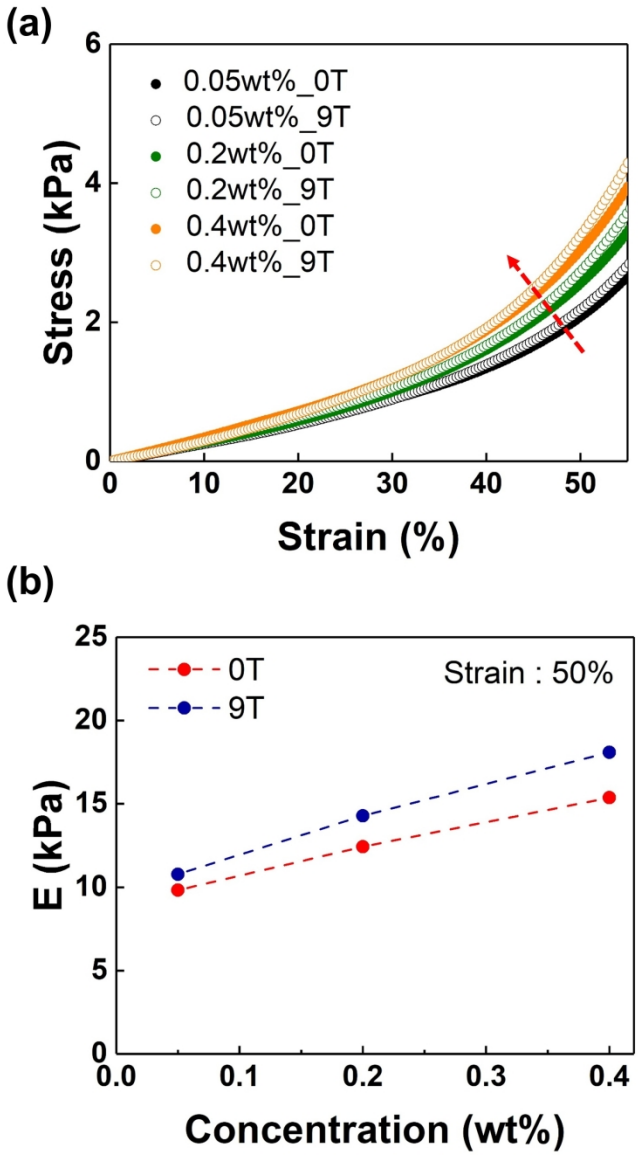

Fig. 7 Mechanical properties of hydrogels prepared in 0 T and 9 T magnetic field strength with different clay concentrations in uniaxial compression test. (a) Stress-strain curves of completely random (0 T) and highly oriented (9 T) hydrogels with different nanoclay concentrations. The red arrow indicates the increase of nanoclay concentration. (Compression direction is parallel to nanoclay orientation direction for 9 T samples) (b) Tangent elastic modulus at 50% strain of hydrogels.

177x304mm (300 x 300 DPI)

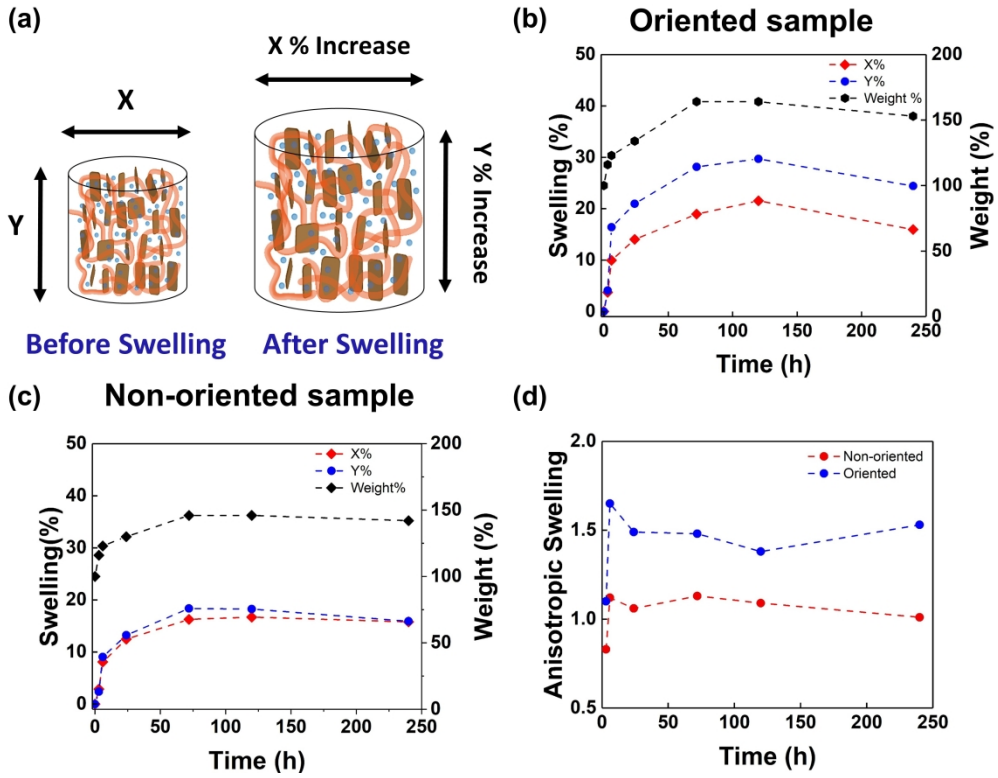

Fig. 8 Swelling behavior of a 0.4wt% clay hydrogels prepared in 0 T and 9 T magnetic field. (a) Schematic illustration of a hydrogel before and after swelling and directions of measurement. Time dependence of the swelling to the radius (X) and thickness (Y) direction along with the weight % increase of (b) the oriented sample and (c) the non-oriented sample. (d) Anisotropic swelling ratio (Y% / X%) of the oriented and non-oriented samples over the swelling time.

360x279mm (300 x 300 DPI)